Water Passivation of Perovskite Nanocrystals Enables Air-Stable Intrinsically Stretchable Color-Conversion Layers for Stretchable Displays

Huanyu Zhou, Jinwoo Park, Yeongjun Lee, Jae-Man Park, Jin-Hoon Kim, Joo Sung Kim, Hyeon-Dong Lee, Seung Hyeon Jo, Xue Cai, Lizhu Li, Xing Sheng, Hyung Joong Yun, Jin-Woo Park, Jeong-Yun Sun, and Tae-Woo Lee*

Conventional organic light-emitting devices without an encapsulation layer are susceptible to degradation when exposed to air, so realization of air-stable intrinsically-stretchable display is a great challenge because the protection of the devices against penetration of moisture and oxygen is even more difficult under stretching. An air-stable intrinsically-stretchable display that is composed of an intrinsically-stretchable electroluminescent device (SELD) integrated with a stretchable color-conversion layer (SCCL) that contains perovskite nanocrystals (PeNCs) is proposed. PeNCs normally decay when exposed to air, but they become resistant to this decay when dispersed in a stretchable elastomer matrix; this change is a result of a compatibility between capping ligands and the elastomer matrix. Counterintuitively, the moisture can efficiently passivate surface defects of PeNCs, to yield significant increases in both photoluminescence intensity and lifetime. A display that can be stretched up to 180% is demonstrated; it is composed of an air-stable SCCL that down-converts the SELD's blue emission and reemits it as green. The work elucidates the basis of moisture-assisted surface passivation of PeNCs and provides a promising strategy to improve the quantum efficiency of PeNCs with the aid of moisture, which allows PeNCs to be applied for air-stable stretchable displays.

Soft materials and processing have enabled development of a wide variety of wearable electronics including on-skin electrical, physical and chemical sensors.[1–5] Continuous monitoring of typical physiological data such as respiration rate, heart rate, contraction/expansion of muscles, and ground reaction forces through the sensors is particularly important for the understanding of human physiology and phenotypes that lead from health to diseases (**Scheme 1**a).[6–10] One of the fundamental units of wearable electronics is a stretchable display that simultaneously visualizes signals from the "bodyNet" and provides feedback to the system.[11–16] However, existing organic and quantum-dot (QD) light-emitting devices are degraded by various molecular interactions with oxygen and water.[17,18] The ultimate goal in production of stretchable displays is to fabricate them directly on stretchable substrates that can be placed in conformal contact on human skin.[19–21]

H. Zhou, J. Park, Dr. Y. Lee, J.-M. Park, J. S. Kim, H.-D. Lee, S. H. Jo, Prof. J.-Y. Sun, Prof. T.-W. Lee
Department of Materials Science and Engineering
Seoul National University
1 Gwanak-ro, Gwanak-gu, Seoul 08826, Republic of Korea
E-mail: twlees@snu.ac.kr
Prof. T.-W. Lee
School of Chemical and Biological Engineering
Seoul National University (SNU)
Seoul 08826, Republic of Korea
Prof. T.-W. Lee
Institute of Engineering Research
Research Institute of Advanced Materials
Nano Systems Institute (NSI)
Seoul National University
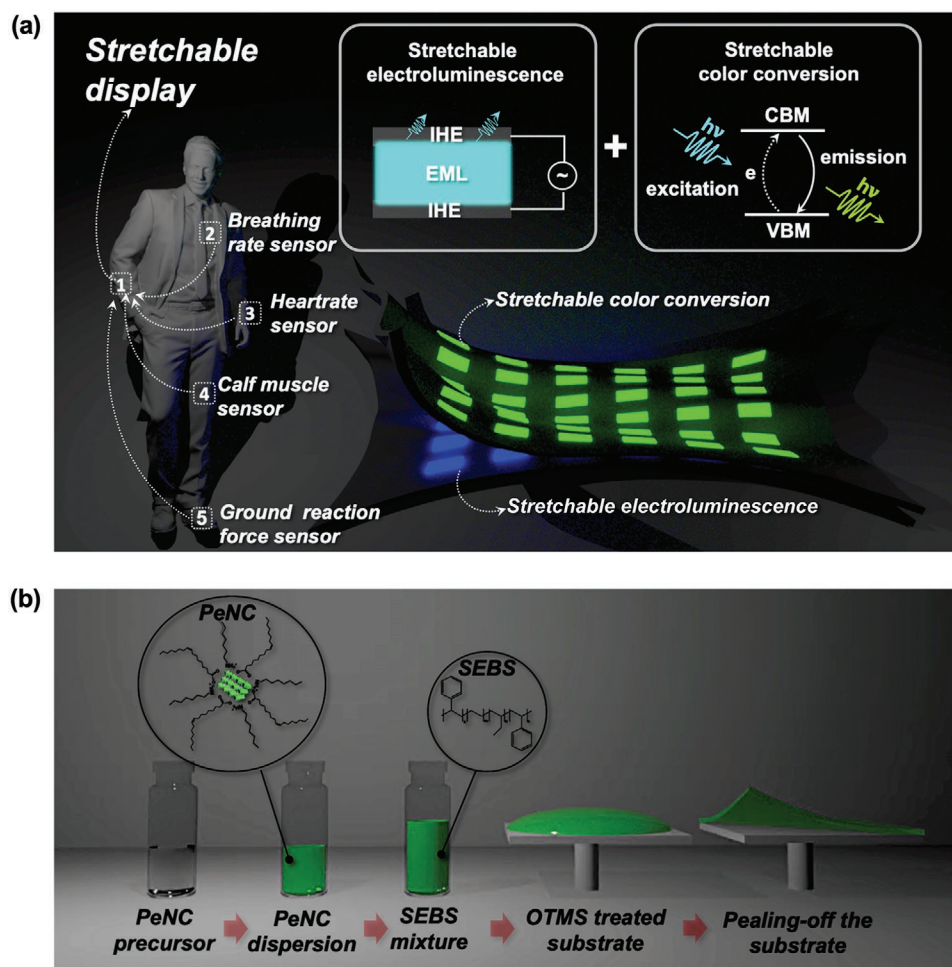1 Gwanak-ro, Gwanak-gu, Seoul 08826, Republic of Korea

J.-H. Kim, Prof. J.-W. Park
Department of Materials Science and Engineering
Yonsei University
Seoul 03722, Republic of Korea
X. Cai, L. Li, Prof. X. Sheng
Department of Electronic Engineering
Tsinghua University
Beijing 100084, China
Dr. H. J. Yun
Advanced Nano Research Group
Korea Basic Science Institute (KBSI)
Daejeon 34126, Republic of Korea

The ORCID identification number(s) for the author(s) of this article can be found under https://doi.org/10.1002/adma.202001989.

**ADVANCED
SCIENCE NEWS**

www.advancedsciencenews.com

**ADVANCED
MATERIALS**

www.advmat.de

Scheme 1. a) Conceptual applications of stretchable displays for visualizing signals from wearable sensors, and 3D schematic of stretchable display that uses a stretchable color conversion layer (SCCL) integrated with a stretchable electroluminescent device (SELD). The inset at left: SELD structure with emitting layer (EML) sandwiched between two ionic hydrogel electrodes (IHEs); inset at right: color conversion mechanism. b) Schematic of experimental procedure to fabricate SCCL using PeNCs, with SEBS as the polymer matrix.

Current stretchable devices require an excellent stretchable encapsulation layer to avoid acceleration of degradation in air during stretching; avoiding the need for an encapsulation layer is currently a serious bottleneck to the development of stretchable displays.[22]

One solution to this problem is to fabricate intrinsically stretchable light-emitting devices that are stable in air without an encapsulation layer. One can combine blue light-emitting devices with a stretchable air-stable color-conversion layer to attain full-color displays: use of air-stable stretchable color-conversion layer (SCCL) can avoid the use of stretchable encapsulation layer and conventional pixelated green-emitting or red-emitting organic and QD devices that are prone to degrade when stretched or exposed to air. Furthermore, the wide linewidth of the emission spectrum of conventional down-conversion phosphors does not meet the requirements for vivid displays.[23] In conventional phosphor-based solid-state white light-emitting diodes (LEDs), the typical device structure fabricated on Si substrate is composed of a blue-emitting gallium nitride (GaN) LED with a coating of Ce^{3+}-doped yttrium aluminum garnet that absorbs a certain fraction of the blue light and re-emits it at a longer wave-

length.[24] In the same manner, the emission wavelength and linewidth of the stretchable electroluminescent device (SELD) can be tailored by using a stretchable color conversion layer and applying it directly to the top of the SELD (Scheme 1a).

Here we demonstrate a simple approach to fabricate an air-stable stretchable display that has a free-standing SCCL and does not require stretchable encapsulation layer. We used methylammonium lead bromide ($MAPbBr_3$) perovskite nanocrystals (PeNCs) combined with styrene-ethylene-butylene-styrene (SEBS). PeNCs degrade rapidly in air; to overcome this limitation, we encapsulated the PeNCs in SEBS matrix to concurrently impart stretchability to the SCCL and to improve its chemical stability. The SCCL down-converts the SELD's blue emission and reemits it as green. PeNCs exhibit remarkable properties such as size-independent narrow spectrum, tunable wavelength, and high photoluminescence quantum yield (PLQY).[25–30] Counterintuitively, we observed that controlled diffusion of moisture through the SEBS polymer matrix into the PeNCs can efficiently passivate their surface defects.

SEBS is a transparent triblock copolymer that has rubber-like elasticity with tensile strength of 10.3–35 MPa and elongation at

break of 500–700%.[31] The elasticity of SEBS originates mainly from phase-separated rigid polysytrene (PS) domains within soft polybutylene and polyethylene middle blocks.[31] Estimates using Hansen solubility parameters suggest that SEBS has high miscibility in oleic acid (Table S1, Supporting Information), and effectively encapsulates the surface of the PeNCs with a long alkyl-chain ligand that stabilizes them when they are dispersed in the SEBS matrix.[11]

MAPbBr$_3$ PeNCs were synthesized using ligand-assisted reprecipitation (Supporting information).[32] As-prepared MAPbBr$_3$ PeNCs were mixed with 100 mg mL^{-1} SEBS solution (1:2 v:v) for 12 h with stirring at 300 rpm in an N$_2$-filled glove box. The solution was spin-cast onto a Si substrate that had been coated with octadecyltrimethoxysiliane (OTMS); the resulting "reference" film was peeled off from the OTMS layer to yield a free-standing SCCL that had a bright-green emission spectrum (Scheme 1b; details in Supporting Information).

To further increase the PeNC loading in the SEBS for color-conversion application, the precipitate after centrifugation was used. We dispersed precipitated PeNCs in 100 mg mL^{-1} SEBS colloidal solution in toluene; our photoluminescence (PL) peaks occurred at 533 nm with an average PLQY of 70.0%. Compared with the reference SCCL, our peaks increasingly red-shifted with increasing PeNC loading in the SEBS (**Figure 1**a). However, the Stokes shift with increase in PeNC loading was <2 nm, which is not significant, and indicates that the optical properties of PeNCs are well preserved. The maximum PL intensity was obtained with 90 mg mL^{-1} PeNCs in the SEBS solution, so this loading is used as the standard SCCL fabrication condition in the remaining experiments and characterizations. The final film thickness was ≈70 µm.

The photostability of PeNCs was evaluated under continuous illumination at wavelength λ = 530 nm (Figure 1b). PeNCs that had been encapsulated in a glass lid lost 23.2% of their PL intensity after 1 h of illumination, whereas those that were not encapsulated lost only ≈10%. When the SCCL was used, the PL intensity initially increased slightly to 105%, then decayed continuously. We hypothesize that the initial increase in photostability may occur because the surfaces of the PeNCs are passivated by oxygen or moisture, or both, in the air.

The response of PL intensity to tensile strain was also evaluated (Figure 1c,d). The PL intensity decreased by 29.8% at 100% tensile strain, but recovered to the initial state when the strain was released. The initial decline occurs because the particle density per unit area decreases during stretching; the recovery occurs because this density returns to its initial level after the strain is released, which can be expressed using the scaling law:[33]

$$I/I_0 \propto \eta/\eta_0 \propto A_0/A \qquad (1)$$

where I is luminance intensity, η is areal number density of phosphors, and A is active area. The scaling law was confirmed by scanning electron microscope (SEM) study of the morphology of SCCL under tensile strain (Figure S1, Supporting Information).

The response of PeNCs to oxygen was measured by passing N$_2$ and O$_2$ alternately for 10 min each at 100 sccm min^{-1} through the PeNC dispersion (Figure S2, Supporting Informa-tion). Increase in oxygen partial pressure led to a decline in PL intensity, because of the strong affinity of oxygen for electrons; direct extraction of photogenerated electrons to oxygen accounts for the oxygen quenching effect.[34] However, this extraction can occur only when O$_2$ molecules are close enough to the surface of PeNCs. Continuous flow of N$_2$ through the dispersion decreased the oxygen partial pressure, and yielded a recovery of PL intensity to the initial state; these observations suggest that oxygen molecules that function as quenching sites were not chemically bonded to the surface of PeNCs. The change in PL intensity was reversible; this result indicates that oxygen is physically adsorbed onto PeNCs without chemical reaction (Figure 1e). This phenomenon precludes the possibility that oxygen can boost the PL intensity during photostability measurement. Hence, the increase in PL intensity might be induced by water-assisted passivation of surface defect.

We propose that PeNC surfaces are passivated at the initial stage, then decompose in a water environment. Therefore, to prolong the passivation and delay the decomposition process, the pristine PeNC film was treated with water vapor, rather than by immersion in water. The sample was stored in a glass container with a small Petri dish filled with deionized water to maintain relative humidity (RH) > 70%. PL and PLQY during the Water vapor treatment (WVT) were measured every 10 min (Figure 1f,g). The PL intensity increased monotonically until 70 min, whereas the PLQY increased from 65.1% to 71.2%.

The SCCL was then immersed in water at room temperature to prove its positive effect on PL intensity (Figure 1h). The peak red-shifted by 2 nm in the SCCL that had been soaked in water for 70 d; this change implies that crystal size had increased,[32] which is also consistent with the following transmission electron microscopy (TEM) results of PeNCs after exposure to moisture (**Figure 2**a). Concurrently, the PL intensity increased by 125% as a consequence of the passivation of surface defects, while the PLQY increased from 70% to 76.3% after 30 d of immersion in water (Figure S3, Supporting Information). We also tested the moisture-assisted passivation effect using PMMA as the matrix to encapsulate the PeNCs; the peak intensity increased by 82% with a redshift from 518 to 522 nm after 12 h of WVT; this result proves that moisture-assisted passivation of PeNCs can be applied to other polymer matrices (Figure S4, Supporting Information). The water-assisted passivation mechanism can be utilized for some other halogen-based PeNCs. FAPbBr$_3$ and mixed-cation MA$_{0.5}$FA$_{0.5}$PbBr$_3$ PeNCs were spin-cast on glass substrate, then treated with water vapor. The PL peak area of FAPbBr$_3$ started to decrease immediately, whereas that of MA$_{0.5}$FA$_{0.5}$PbBr$_3$ increased by 22.3% after 5 min WVT; this result suggests that the passivation effect is dependent on the type of cation used in the PeNCs (Figure S5, Supporting Information).

Generally, PeNCs are vulnerable to water because of a dynamic interaction between ligands and nanocrystals.[35,36] A minor amount of water can be introduced to the precursor solutions during the synthesis process; the water forms an inorganic matrix that entirely wraps the perovskites and efficiently passivates the surface defects.[37,38] In addition, ionized water molecules can partially replace surface ligands and affect the preferred growth orientation, so the size and shape of PeNCs can also be correlated with the water content.[39] However, these

ADVANCED
SCIENCE NEWS
www.advancedsciencenews.com

ADVANCED
MATERIALS
www.advmat.de
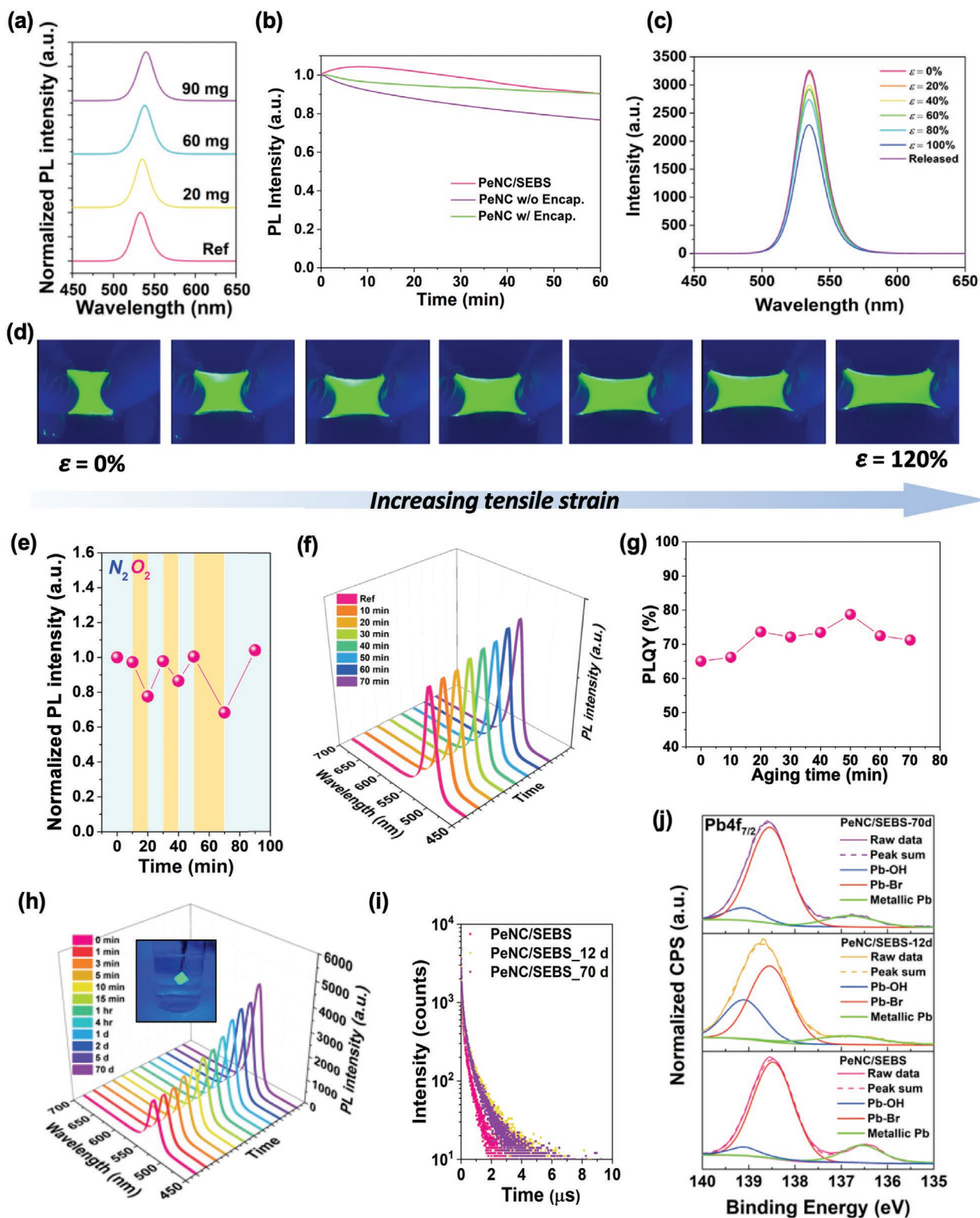
Figure 1. a) PL spectra with the addition of PeNCs to SEBS matrix. b) Photostability of PeNC/SEBS composites and PeNCs thin films with or without encapsulation. c) Evolution of PL spectra and d) photographic images of the SCCL under uniaxial tensile strain. e) Evolution of PL peak intensity of PeNC solution under alternating flow of O_2 and N_2 at 100 sccm min^{-1}. Evolution of f) PL spectra and g) PLQY of spin-cast PeNCs thin film during water vapor treatment (WVT, RH ≈ 70%) up to 70 min. h) Evolution of PL spectra of SCCL after immersion in deionized water (DIW) for up to 70 d; inset: photograph of the SCCL in the DIW. i) TCSPC spectra of pristine PeNC/SEBS before and after immersion in DIW after 12 and 70 d. j) XPS of Pb4f7/2 of PeNC/SEBS composite before and after immersion in DIW for 12 and 70 d.
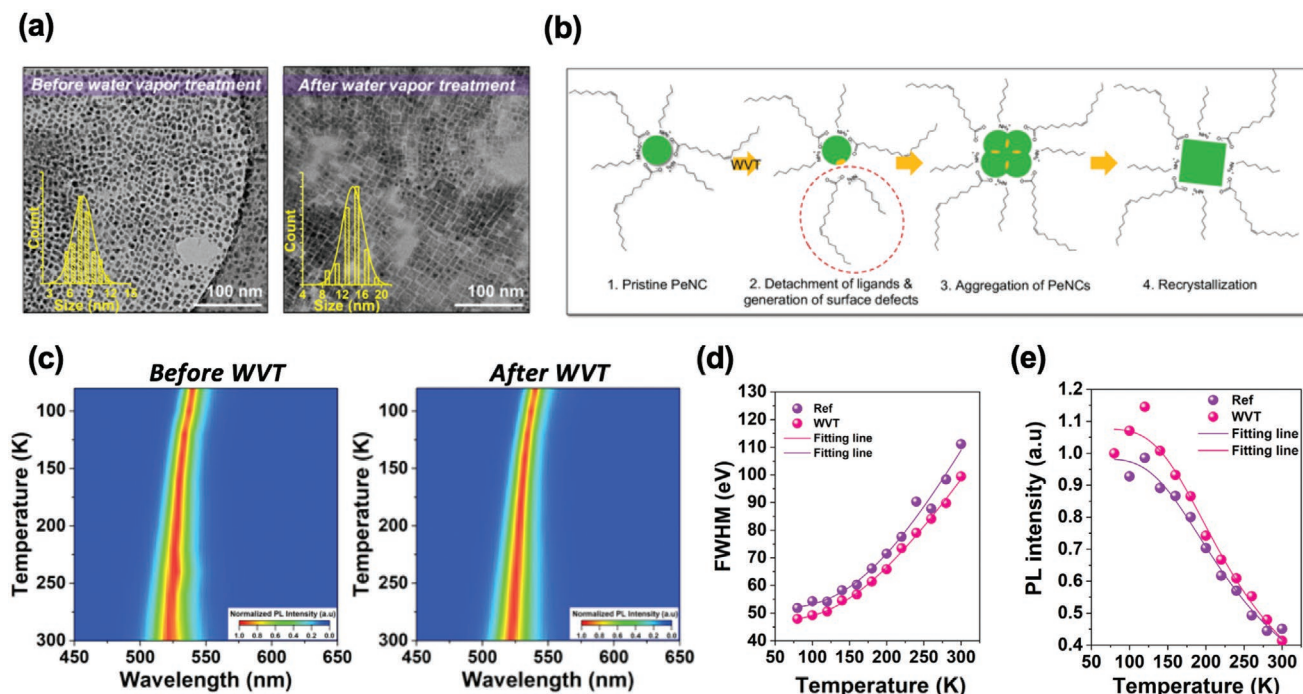
Figure 2. High-resolution transmission electron microscopy (HR-TEM) and fast Fourier transform (FFT) images of PeNCs a) before and after the water-vapor treatment (WVT). b) Schematic illustration of formation process of platelet structure. c) Color plots of normalized steady-state PL for PeNCs before and after WVT at temperatures of 80–300 K in increments of 20 K. Evolution of d) PL intensity and e) full width at half maximum (FWHM) as the function of temperature deduced from the same spectra.

processes yield a rigid inorganic matrix, which is not appropriate for stretchable applications.

Therefore, in this study, the nanocrystals (PeNCs) were first synthesized and then re-dispersed in SEBS elastomer matrix. Controlled diffusion of moisture through this matrix can effectively passivate surface defects that quench excitons. WVT of bulk perovskite is widely adopted to improve the optical and electrical properties of polycrystalline perovskite thin film for solar cells,[40] but this is the first report of post-synthesis moisture-assisted surface passivation of PeNCs particles.

Time-correlated single photon counting of the SCCL during immersion in water (Figure 1i) demonstrated that the PL decay over time can be described well by a triexponential model. The average PL lifetimes of the sample were 368.3 ns before immersion, 737.7 ns after immersion for 12 d, and 599.8 ns after immersion for 70 d (Table S2, Supporting Information). The initial increase in PL lifetime during immersion indicates a decrease in the number of surface defects that function as nonradiative recombination sites. The decrease in PL lifetime at 70 d suggests that extensive immersion of PeNCs in water would in turn degrade themselves. This originated from failing to control the diffusion rate of moisture through the polymer matrix due to the increase in amount of residual water molecules.[41]

High-resolution X-ray photoelectron spectroscopy (XPS) was conducted to further analyze the chemical state of SCCL before and after the water stability test. The Pb 4f7/2 spectrum for the SCCL recorded three contributions: metallic Pb at 136.5 eV, the Pb−Br bond at 138.5 eV, and the Pb−OH bond at 139.1 eV (Figure 1j).[42] Metallic Pb atoms strongly quench excitons and must be eliminated using stoichiometric engineering in the case of bulk perovskites.[43] However, the metallic Pb peak of

the SCCL was eliminated after immersion in water; the O1s spectrum showed the Pb–OH peak at 531.5 eV (Figure S6, Supporting Information); this result indicates that the Pb atoms oxidized to form Pb–OH bonds. The Pb–OH intensity decreased after extensive soaking in water for 70 d due to higher diffusion of moisture through the swollen polymer matrix.

The structural evolution of PeNCs films during the WVT was studied using x-ray diffraction spectroscopy (Figure S7, Supporting Information). The spectra did not show shifts in the peaks; this lack of change indicates that no phase transition occurred. However, PeNC shape changed from spherical to platelet after 50 min of WVT, and TEM showed that the average particle size increased from 7.9 to 14.1 nm (Figure 2a).

We propose the following mechanism to explain the formation of platelet structure after WVT (Figure 2b). Given the fact that water is a polar solvent, it can be ionized into H_3O^+ and OH^- that can partially replace surface ligands and affect the preferred growth orientation.[39] Once the moisture diffuses through the SEBS matrix and arrives at the surface of the PeNCs, their ionic ligands can be captured by the polar H_2O molecules and readily removed from the PeNC surface, creating the surface without capping ligands. Therefore, PeNCs tend to aggregate with their neighbors and reconstruct the surface to reduce the total energy.

The PeNCs thin films before and after WVT were further characterized using steady-state PL spectra at temperatures from 80 to 300 K in increments of 20 K (Figure 2c). The normalized PL spectra of the same PeNCs for the whole temperature range (Figure S8, Supporting Information) differ from those of inorganic semiconductors. In PeNCs, the band gap is determined by the boundary of the Brillouin zone; the band

**ADVANCED
SCIENCE NEWS**

www.advancedsciencenews.com

**ADVANCED
MATERIALS**

www.advmat.de
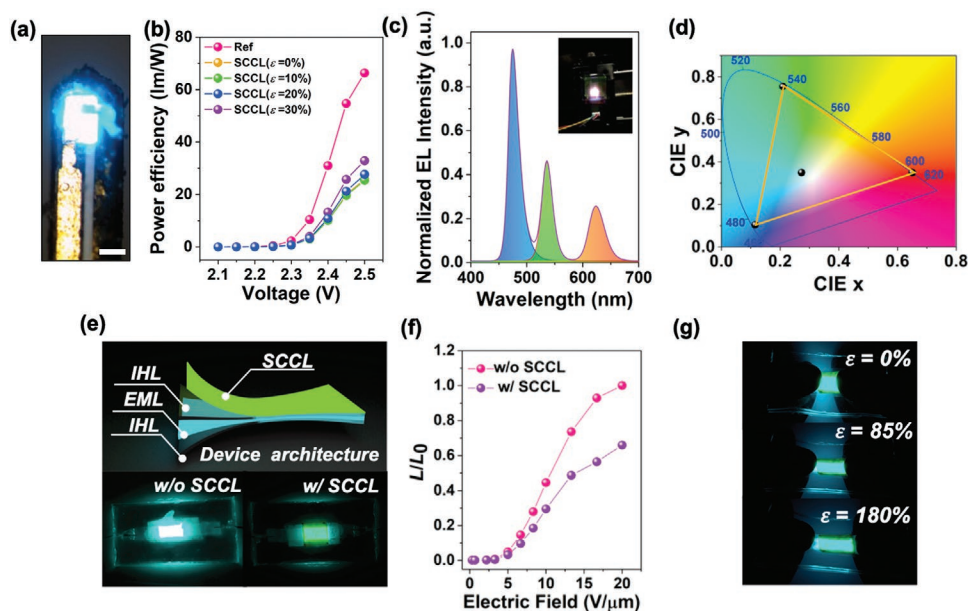
Figure 3. a) Optical microscope images of μ-LED with DC voltage of 2.3 V. Scale bar: 200 μm. b) power efficiency (lm W^{-1}) before and after integration of SCCL, to maximum tensile strain of 30%. c) EL spectrum of μ-LED integrated with bilayer SCCL composed of CdSe/ZnS and MAPbBr$_3$ PeNCs for white emission. d) CIE coordinates of device in (c). e) Device structure and photographic images of SELDs during stretching before and after integration with SCCL. f) Normalized luminance of SELD before and after integration with SCCL. g) Photographs of SELD integrated with the SCCL under tensile strain up to 180%.

gap-edge states stabilize as the lattice expands, so the band-gap energy increases as temperature increases.[44]

The temperature dependence of PL linewidth can be exploited to study the electron-phonon scattering that is responsible for the nonradiative decay of excitons (Figure 2d). The linewidth broadens as absolute temperature T increases:[45]

$$\Gamma(T) = \Gamma_0 + \Gamma_{ac} + \Gamma_{LO} = \Gamma_0 + \gamma_{ac}T + \gamma_{LO}N_{LO}(T) \quad (2)$$

where $\Gamma(T)$ is a temperature-dependent inhomogeneous term that arises from disorder and imperfections; Γ_{ac} and Γ_{LO} represent respectively homogenous broadening induced by acoustic and longitudinal optical (LO) phonons, and γ_{ac} and γ_{LO} are their corresponding coupling strengths, respectively; $N_{LO}(T)$ is the Bose–Einstein distribution function that describes the occupation numbers of the respective LO phonons. Comparison of γ_{ac} and γ_{LO} indicates that the acoustic phonon coupling by the deformation potential interaction is not dominant for PeNCs either before or after WVT; this conclusion is in accordance with previous results (Table S3, Supporting Information).[45,46] After WVT, γ_{LO} decreased from 368.3 to 246.5 meV; this change indicates that the number of non-radiative pathways decreased. Moreover, the Urbach energy extracted from the absorption spectra at the band edge decreased as WVT duration was increased to 60 min (Figure S9, Supporting Information); this trend implies a decrease in electronic disorder such as defects that quench excitons. Hence, we conclude that WVT indeed passivates the surface of the PeNCs without the aid of the elastomer matrix, and thereby yields an increase in PLQY.

PL intensity decreased exponentially as temperature increased (Figure 2e); this trend is a result of competition between exciton dissociation and radiative recombination. $I(T)$ can be fitted to the Arrhenius equation as

$$I(T) = I_0 / \left[1 + A \cdot \exp\left(-E_a / (k_B T)\right) \right] \quad (3)$$

where I_0 (eV) is PL intensity at 0 K, E_a (eV) is the activation energy for exciton dissociation (exciton binding energy), A (scalar) is a pre-exponential coefficient, and $k_B = 8.617 \times 10^{-5}$ eV J^{-1} is the Boltzmann constant. After WVT, E_a increased from 64.50 to 70.91 meV, which is consistent with the decrease in dielectric constant as indicated in the capacitance–frequency (C–f) curve (Figure S10, Supporting Information).[47]

To assess the color-converting property of the SCCL, a high-efficiency blue-emitting micro-scale light-emitting diode (μ-LED) ($\lambda_{max} = 476$ nm) based on gallium nitride was fabricated on flexible polyimide substrate, then used to convert colors (**Figure 3**a). The green SCCL was applied to the top of the blue μ-LED to convert the blue light from the device to a green emission (Figure 3b). We normalize the EL spectrum first based on the blue peak intensity, then measured the SCCL's color-conversion efficiency (η) is calculated using the photon energy, which is defined as $\int I_{Green}(\lambda)(hc/\lambda)d\lambda / \int I_{Blue}(\lambda)(hc/\lambda)d\lambda$, where I_{Green}, and I_{Blue} represent the intensity of the green and blue light at a certain wavelength in the EL spectrum, λ is the photon's wavelength, h is the Planck constant, and c is the speed of light in vacuum. As the number of stacked SCCL layers increased from one to three, η increased from 11.58% to 95.36% with applying 2.6 V to the μ-LED (Figure S11, Supporting Information).

We also assessed the response of an organic photodiode (OPD) during illumination of μ-LED with varying numbers of SCCL layers (Figure S12, Supporting Information). The absorbance of the active layer of the OPD is higher at $\lambda = 467$ nm than

at $\lambda = 538$ nm, so the increase in I_G/I_B ratio will lead to decrease in responsivity of the OPD, that is, the current I_L under illumination versus current I_D in darkness (Table S4, Supporting Information). To achieve white emission, a red SCCL composed of CdSe/ZnS and SEBS was fabricated using the same method, then transferred directly onto the green-emitting SCCL that used of MAPbBr$_3$ PeNCs (Figure 3c). The PL peak positions of primary colors were 474.6, 535.7, and 623.2 nm, respectively. CIE coordinates of the three primary colors were (0.11, 0.10), (0.21, 0.75), and (0.65, 0.35) (Figure 3d). This chromaticity triangle area indicates that this device has potential applications in vivid stretchable displays with a color gamut ratio of 103.03% based on the NTSC standard.

The coordinate could be placed anywhere on the chart by modulating the stacking order of red and green SCCLs and number of layers. The white emission generated from the red and green SCCL was located at (0.28, 0.35) with the color correlated temperature of 8049 K.

Finally, the SCCL was integrated with an SELD for stretchable display application. The challenge of the intrinsically stretchable light-emitting device is to maintain the device function while it is under large tensile strain. We used an ionic hydrogel electrode (IHE) made of polyacrylamide and NaCl as the electrode, and ZnS:Cu/PDMS composite as the stretchable emitting layer (EML) of an alternating-current electroluminescent device (Figure 3e). The stress–strain curve of the IHE was measured using a tensile test; the IHE had Young's modulus of 10.8 kPa, and elongation at break of 1400% (Figure S13, Supporting Information).

Instant bonding at the interface between the IHE and the EML or SCCL without forming a rigid resin interlayer was achieved using ethyl cyanoacrylate as the bonding agent.[48] The EL intensity L in cd increased exponentially as bias voltage V was increased, as

$$L = L_0 \exp\left(-\beta/V^{1/2}\right) \tag{4}$$

where initial EL intensity L_0 in cd and decay-rate factor β are constants that vary among devices.[49] Immediately after integration of the SCCL, the blue-light emission (CIE coordinate (0.175, 0.388)) from the SELD change to green (0.238, 0.568), while the maximum EL intensity at 20 V μm^{-1} decreased by 34% (Figure 3f). When the SELD was manually stretched up to 180% strain, the EL intensity showed negligible change; this stability indicate that strong bonds formed at both the IHE/EML and the SCCL/IHE interfaces (Figure 3g). Furthermore, the devices showed a negligible change (<3%) in EL intensity after 1 h continuous operation under an AC electric field of 10 V μm^{-1} and after 30 d-storage in ambient air (RH ≈ 40%, ≈18 °C) (Figure S14, Supporting Information).

In conclusion, this work has reported an air-stable stretchable display that is composed of a SELD and an air-stable PeNC SCCL that down-converts the blue emission from the SELD to green light. PeNCs were stabilized using a SEBS polymer matrix that can effectively encapsulate the surface of PeNCs, and thereby significantly increase their stability in air. Notably, the SCCL recovered its original PL intensity after being stretched to 100% tensile strain, then released. During a test of stability during immersion in water, the PL intensity of the SCCL increased to 225% after 70 d; this is the first observation of moisture-assisted surface passivation of PeNC emitters unlike organic emitters and conventional inorganic quantum dots. The increased PL intensity of the SCCL is attributable to oxidation of metallic Pb atoms that quench excitons, combined with formation of platelet structure with decreased numbers of surface defects. By blending nanocrystals with different re-emission wavelengths with SEBS polymer, we achieved white emission by a blue μ-LED. We also fabricated an air-stable intrinsically stretchable display that is composed of an SCCL and intrinsically stretchable blue electroluminescent devices. Our strategy to make air-stable stretchable displays without using any stretchable encapsulation layer is superior to the conventional approach of using intrinsically stretchable organic light-emitting devices that essentially require a stretchable encapsulation layer with low water vapor transmission rate under stretching.

Supporting Information

Supporting Information is available from the Wiley Online Library or from the author.

Conflict of Interest

The authors declare no conflict of interest.

[1] T. Someya, M. Amagai, *Nat. Biotechnol.* **2019**, *37*, 382.
[2] S. Bauer, *Nat. Mater.* **2013**, *12*, 871.
[3] Y. Wang, C. Zhu, R. Pfattner, H. Yan, L. Jin, S. Chen, F. Molina-Lopez, F. Lissel, J. Liu, N. I. Rabiah, Z. Chen, J. W. Chung, C. Linder, M. F. Toney, B. Murmann, Z. Bao, *Sci. Adv.* **2017**, *3*, e1602076.
[4] N. Liu, A. Chortos, T. Lei, L. Jin, T. R. Kim, W.-G. Bae, C. Zhu, S. Wang, R. Pfattner, X. Chen, R. Sinclair, Z. Bao, *Sci. Adv.* **2017**, *3*, e1700159.

**ADVANCED
SCIENCE NEWS**

www.advancedsciencenews.com

**ADVANCED
MATERIALS**

www.advmat.de

[5] M. Park, J. Im, M. Shin, Y. Min, J. Park, H. Cho, S. Park, M.-B. Shim, S. Jeon, D.-Y. Chung, J. Bae, J. Park, U. Jeong, K. Kim, *Nat. Nanotechnol.* **2012**, *7*, 803.

[6] D. J. Lipomi, M. Vosgueritchian, B. C. K. Tee, S. L. Hellstrom, J. A. Lee, C. H. Fox, Z. Bao, *Nat. Nanotechnol.* **2011**, *6*, 788.

[7] J. Y. Oh, D. Son, T. Katsumata, Y. Lee, Y. Kim, J. Lopez, H.-C. Wu, J. Kang, J. Park, X. Gu, J. Mun, N. G.-J. Wang, Y. Yin, W. Cai, Y. Yun, J. B.-H. Tok, Z. Bao, *Sci. Adv.* **2019**, *5*, eaav3097.

[8] S. H. Kim, H. Seo, J. Kang, J. Hong, D. Seong, H.-J. Kim, J. Kim, J. Mun, I. Youn, J. Kim, Y.-C. Kim, H.-K. Seok, C. Lee, J. B. H. Tok, Z. Bao, D. Son, *ACS Nano* **2019**, *13*, 6531.

[9] Y. Zheng, G.-J. N. Wang, J. Kang, M. Nikolka, H.-C. Wu, H. Tran, S. Zhang, H. Yan, H. Chen, P. Y. Yuen, J. Mun, R. H. Dauskardt, I. McCulloch, J. B.-H. Tok, X. Gu, Z. Bao, *Adv. Funct. Mater.* **2019**, *29*, 1905340.

[10] M. Shin, J. H. Song, G.-H. Lim, B. Lim, J.-J. Park, U. Jeong, *Adv. Mater.* **2014**, *26*, 3706.

[11] B. Chu, W. Burnett, J. W. Chung, Z. Bao, *Nature* **2017**, *549*, 328.

[12] S. Lee, D. Sasaki, D. Kim, M. Mori, T. Yokota, H. Lee, S. Park, K. Fukuda, M. Sekino, K. Matsuura, T. Shimizu, T. Someya, *Nat. Nanotechnol.* **2019**, *14*, 156.

[13] J. Y. Oh, S. Rondeau-Gagné, Y.-C. Chiu, A. Chortos, F. Lissel, G.-J. N. Wang, B. C. Schroeder, T. Kurosawa, J. Lopez, T. Katsumata, J. Xu, C. Zhu, X. Gu, W.-G. Bae, Y. Kim, L. Jin, J. W. Chung, J. B. H. Tok, Z. Bao, *Nature* **2016**, *539*, 411.

[14] J. Kang, D. Son, G.-J. N. Wang, Y. Liu, J. Lopez, Y. Kim, J. Y. Oh, T. Katsumata, J. Mun, Y. Lee, L. Jin, J. B.-H. Tok, Z. Bao, *Adv. Mater.* **2018**, *30*, 1706846.

[15] J. S. Kim, S. H. Cho, K. L. Kim, G. Kim, S. W. Lee, E. H. Kim, B. Jeong, I. Hwang, H. Han, W. Shim, T.-W. Lee, C. Park, *Nano Energy* **2019**, *59*, 773.

[16] E. H. Kim, H. Han, S. Yu, C. Park, G. Kim, B. Jeong, S. W. Lee, J. S. Kim, S. Lee, J. Kim, J.-U. Park, W. Shim, C. Park, *Adv. Sci.* **2019**, *6*, 1802351.

[17] H. Moon, C. Lee, W. Lee, J. Kim, H. Chae, *Adv. Mater.* **2019**, *31*, 1804294.

[18] S. Scholz, D. Kondakov, B. Lüssem, K. Leo, *Chem. Rev.* **2015**, *115*, 8449.

[19] S. Wang, J. Xu, W. Wang, G.-J. N. Wang, R. Rastak, F. Molina-Lopez, J. W. Chung, S. Niu, V. R. Feig, J. Lopez, T. Lei, S.-K. Kwon, Y. Kim, A. M. Foudeh, A. Ehrlich, A. Gasperini, Y. Yun, B. Murmann, J. B. H. Tok, Z. Bao, *Nature* **2018**, *555*, 83.

[20] Y. Lee, J. Y. Oh, T. R. Kim, X. Gu, Y. Kim, G.-J. N. Wang, H.-C. Wu, R. Pfattner, J. W. F. To, T. Katsumata, D. Son, J. Kang, J. R. Matthews, W. Niu, M. He, R. Sinclair, Y. Cui, J. B.-H. Tok, T.-W. Lee, Z. Bao, *Adv. Mater.* **2018**, *30*, 1704401.

[21] J. Y. Oh, Z. Bao, *Adv. Sci.* **2019**, *6*, 1900186.

[22] M.-H. Park, J.-Y. Kim, T.-H. Han, T.-S. Kim, H. Kim, T.-W. Lee, *Adv. Mater.* **2015**, *27*, 4308.

[23] Y.-C. Huang, T.-C. Lu, C.-I. Huang, *Polymer* **2013**, *54*, 6489.

[24] S. Pathak, N. Sakai, F. Wisnivesky Rocca Rivarola, S. D. Stranks, J. Liu, G. E. Eperon, C. Ducati, K. Wojciechowski, J. T. Griffiths, A. A. Haghighirad, A. Pellaroque, R. H. Friend, H. J. Snaith, *Chem. Mater.* **2015**, *27*, 8066.

[25] H. Cho, Y.-H. Kim, C. Wolf, H.-D. Lee, T.-W. Lee, *Adv. Mater.* **2018**, *30*, 1704587.

[26] Y.-H. Kim, H. Cho, T.-W. Lee, *Proc. Natl. Acad. Sci. USA* **2016**, *113*, 11694.

[27] Y. Kim, E. Yassitepe, O. Voznyy, R. Comin, G. Walters, X. Gong, P. Kanjanaboos, A. F. Nogueira, E. H. Sargent, *ACS Appl. Mater. Interfaces* **2015**, *7*, 25007.

[28] J. Pan, L. N. Quan, Y. Zhao, W. Peng, B. Murali, S. P. Sarmah, M. Yuan, L. Sinatra, N. M. Alyami, J. Liu, E. Yassitepe, Z. Yang, O. Voznyy, R. Comin, M. N. Hedhili, O. F. Mohammed, Z. H. Lu, D. H. Kim, E. H. Sargent, O. M. Bakr, *Adv. Mater.* **2016**, *28*, 8718.

[29] Q. Zhou, Z. Bai, W.-g. Lu, Y. Wang, B. Zou, H. Zhong, *Adv. Mater.* **2016**, *28*, 9163.

[30] M. Meyns, M. Perálvarez, A. Heuer-Jungemann, W. Hertog, M. Ibáñez, R. Nafria, A. Genç, J. Arbiol, M. V. Kovalenko, J. Carreras, A. Cabot, A. G. Kanaras, *ACS Appl. Mater. Interfaces* **2016**, *8*, 19579.

[31] B. Wang, A. Facchetti, *Adv. Mater.* **2019**, *31*, 1901408.

[32] Y.-H. Kim, C. Wolf, Y.-T. Kim, H. Cho, W. Kwon, S. Do, A. Sadhanala, C. G. Park, S.-W. Rhee, S. H. Im, R. H. Friend, T.-W. Lee, *ACS Nano* **2017**, *11*, 6586.

[33] C. Larson, B. Peele, S. Li, S. Robinson, M. Totaro, L. Beccai, B. Mazzolai, R. Shepherd, *Science* **2016**, *351*, 1071.

[34] M. Lorenzon, L. Sortino, Q. Akkerman, S. Accornero, J. Pedrini, M. Prato, V. Pinchetti, F. Meinardi, L. Manna, S. Brovelli, *Nano Lett.* **2017**, *17*, 3844.

[35] J. De Roo, M. Ibáñez, P. Geiregat, G. Nedelcu, W. Walravens, J. Maes, J. C. Martins, I. Van Driessche, M. V. Kovalenko, Z. Hens, *ACS Nano* **2016**, *10*, 2071.

[36] A. Pan, B. He, X. Fan, Z. Liu, J. J. Urban, A. P. Alivisatos, L. He, Y. Liu, *ACS Nano* **2016**, *10*, 7943.

[37] K.-K. Liu, Q. Liu, D.-W. Yang, Y.-C. Liang, L.-Z. Sui, J.-Y. Wei, G.-W. Xue, W.-B. Zhao, X.-Y. Wu, L. Dong, C.-X. Shan, *Light: Sci. Appl.* **2020**, *9*, 44.

[38] Z.-Z. Ma, Z.-F. Shi, L.-T. Wang, F. Zhang, D. Wu, D.-W. Yang, X. Chen, Y. Zhang, C.-X. Shan, X.-J. Li, *Nanoscale* **2020**, *12*, 3637.

[39] X. Zhang, X. Bai, H. Wu, X. Zhang, C. Sun, Y. Zhang, W. Zhang, W. Zheng, W. W. Yu, A. L. Rogach, *Angew. Chem., Int. Ed.* **2018**, *57*, 3337.

[40] A. M. A. Leguy, Y. Hu, M. Campoy-Quiles, M. I. Alonso, O. J. Weber, P. Azarhoosh, M. van Schilfgaarde, M. T. Weller, T. Bein, J. Nelson, P. Docampo, P. R. F. Barnes, *Chem. Mater.* **2015**, *27*, 3397.

[41] G. Rainò, A. Landuyt, F. Krieg, C. Bernasconi, S. T. Ochsenbein, D. N. Dirin, M. I. Bodnarchuk, M. V. Kovalenko, *Nano Lett.* **2019**, *19*, 3648.

[42] Y. Cao, A. Stavrinadis, T. Lasanta, D. So, G. Konstantatos, *Nat. Energy* **2016**, *1*, 16035.

[43] H. Cho, S.-H. Jeong, M.-H. Park, Y.-H. Kim, C. Wolf, C.-L. Lee, J. H. Heo, A. Sadhanala, N. Myoung, S. Yoo, S. H. Im, R. H. Friend, T.-W. Lee, *Science* **2015**, *350*, 1222.

[44] Y. Chen, N. Li, L. Wang, L. Li, Z. Xu, H. Jiao, P. Liu, C. Zhu, H. Zai, M. Sun, W. Zou, S. Zhang, G. Xing, X. Liu, J. Wang, D. Li, B. Huang, Q. Chen, H. Zhou, *Nat. Commun.* **2019**, *10*, 1112.

[45] A. D. Wright, C. Verdi, R. L. Milot, G. E. Eperon, M. A. Pérez-Osorio, H. J. Snaith, F. Giustino, M. B. Johnston, L. M. Herz, *Nat. Commun.* **2016**, *7*, 11755.

[46] C. Wolf, T.-W. Lee, *Mater. Today Energy* **2018**, *7*, 199.

[47] X. Sun, C. Han, K. Wang, H. Yu, J. Li, K. Lu, J. Qin, H. Yang, L. Deng, F. Zhao, Q. Yang, B. Hu, *ACS Appl. Energy Mater.* **2018**, *1*, 6992.

[48] D. Wirthl, R. Pichler, M. Drack, G. Kettlguber, R. Moser, R. Gerstmayr, F. Hartmann, E. Bradt, R. Kaltseis, C. M. Siket, S. E. Schausberger, S. Hild, S. Bauer, M. Kaltenbrunner, *Sci. Adv.* **2017**, *3*, e1700053.

[49] J. Wang, C. Yan, K. J. Chee, P. S. Lee, *Adv. Mater.* **2015**, *27*, 2876.

2001989 (8 of 8)